Engineering Structures 147 (2017) 625–638

Contents lists available at ScienceDirect

Engineering Structures

journal homepage: www.elsevier.com/locate/engstruct

Experimental study on interior connections in modular steel buildings

Zhihua Chen [a,b], Jiadi Liu [b], Yujie Yu [b,*]

[a] State Key Laboratory of Hydraulic Engineering Simulation and Safety, Tianjin, China
[b] Department of Civil Engineering, Tianjin University, Tianjin, China

ARTICLE INFO

Article history:
Received 18 November 2016
Revised 31 May 2017
Accepted 2 June 2017

Keywords:
Inter-module connection
Plug-in device
Beam-to-beam bolted connection
Monotonic test
Quasi-static cyclic test

ABSTRACT

In modular steel buildings, traditional architectures are separated into prefabricated room-sized volumetric units that are manufactured offsite and installed onsite. The connections between the modules are important for load transfer. Conventional inter-module connections mainly use direct plates and connect them using bolts; however, this may prove problematic for the inner connecting regions. A new type of design with beam-to-beam bolted connections is proposed in this paper; this design provides easy working access without being affected by the structural members. The static performance, hysteretic performance, skeleton curves, ductile performance, energy dissipation capacity, and stiffness degradation patterns of the joints are obtained by experiments and finite element analyses. The results showed that because of the construction between two unit joints, gaps would be formed between the upper and bottom columns, and this gap can influence the deformation patterns and distribution of bending loads at each unit joint. The weld quality at the unit joints is critical to ensure overall safety. Stiffeners can effectively increase the stiffness and load bearing capacity, but may reduce ductility performance. The deforming ability of the connection is also closely influenced by the stiffness of the floor beam column joint and ceiling beam column joint and their relative intermediate magnitudes.

1. Introduction

Modular construction involves an assembled structure in which the entire structure or building comprises prefabricated room-sized volumetric units or structural units that are manufactured offsite and installed onsite [1]. The modular units are often fully equipped with the required facilities and transported to the construction site; then they are connected onsite to form a complete and permanent residential or commercial building [2] (Fig. 1(a)). Compared to the conventional construction approaches, the off-site modular construction replaces the slow unproductive site activities by more efficient and faster factory processes. The perceived benefits of off-site manufacture are speed of construction, higher quality, lower cost, less wastage, and higher reliability [3]. Further, the modular steel structures are especially suitable for industrial production [4]. In recent years, off-site modular construction has been receiving increasing attention in high-density urban areas, where the construction practices are often constrained by limited working spaces and high requirements on low disturbance during operations [5]. In general, there are mainly two types of modules: continuous four-side support modules where the vertical loads are transmitted through the walls, and corner-supported modules where the vertical loads are transmitted through the corner and intermediate posts. The structural skeleton of the four-side support module mainly comprises light steel C-sections inside the walls, and is normally used for low-rise modular buildings, while the corner-supported modular form often uses hot rolled steel members that can withstand larger vertical loads in mid-rise or high-rise buildings.

Furthermore, these module forms have the units connected at their corners, so that they can structurally work together to transfer wind loads and to provide an alternative load path in the case of damage to a single module [6]. Lawson introduced the common bolted connection method normally used in the UK, and displayed the application exploration of high-rise modular steel buildings (MSBs) [1,6]. The corner columns or angles in adjacent modular units are normally connected together with single bolted connector plates or side plates [7,8]. Lee [9] later reported a rigid connection between vertically adjacent modules, through an extended bracket end at the lower ceiling beam to ensure fastening of bolts to the upper floor beams. Annan [4,10,11] presented a welded inter-module connection design with the upper and lower modular columns directly welded together, and performed seismic evaluation of the welded corner-supported MSBs. Using a similar method,

* Corresponding author at: School of Civil Engineering, Tianjin University, Tianjin, China.
E-mail address: yujietju@tju.edu.cn (Y. Yu).

http://dx.doi.org/10.1016/j.engstruct.2017.06.002
0141-0296/

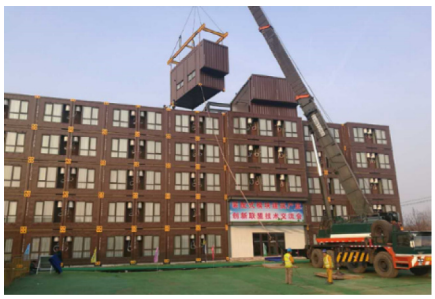

(a) Mid-rise modular residences at Tianjin

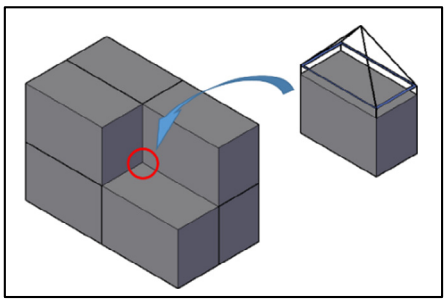

(b) Inner connecting locations of modules groups

Fig. 1. Inner connection characteristics of modular construction.

Fathieh [12] also conducted seismic evaluation of MSBs having bolted steel plates as the inter-module connections. However, most of the reports or references cover only the connecting styles or simplification methods, with limited information on the mechanical performance of the inter-module connections.

At present, most of the (MSBs) have a single array arrangement or a simple layout in which most of the inter-module connections would be located in the perimeter region [13,14]. However, for the inner connections, as shown in Fig. 1(b), the fourth module to be placed cannot be easily connected at its base, unless there is enough working access or a special opening. The modular construction features; its convent on-site erection assembly, and a safe and convenient inter-module connection is needed. In the present paper, a new type of inter-module design for the inner connecting regions is proposed. A series of static and cyclic loading tests were performed to understand the load bearing mechanism and seismic behaviour of the structure. The results can provide useful guidance and serve as reference to modular building design in the future.

2. Details of the new interior inter-module connection

Conventional inter-module connections consist of plates and bolts that are welded from outside; they often require certain space to facilitate bolting or welding. As shown in Fig. 2(a), the horizontally arranged modular units are connected through side plates, and the vertical modules are connected with long stay bolts. For perimeter connections, the connecting work can be performed from outside of the building, and hence there would be no requirement of working space and construction gap. However, for the parts in the central region, the inter-module connections may pose difficulties where four modular units are to be joined together. These connections are installed sequentially as each module is placed, but the fourth module to be placed will not have access to the connection, as shown in Fig. 2(a). One possible solution is to create a working opening in the modular column, but this would cause significant weakening of the structural member. Another approach would be to get working access through a service riser or from infill walls. This method also requires a gap between the modular columns and beams to allow the mechanical and electrical facilities pass through, but such a space is normally not allowed in architectural practice.

The construction and assembly method of the proposed inter-module connection is shown in Fig. 2(b). The new MSB has separate vertical and horizontal connecting systems, which comprise cast plug-in devices for horizontal connections and the beam-to-beam high tensile strength bolting system for vertical connections. When the modular buildings are of corner-support type, each inner MSB connection will have four unit joints. All the modular beams and columns are made of cold formed rectangular steel tubes, and the small beams and columns in each unit joint are connected through welding. The connection has a cover plate welded to the upper floor beam, and an intermediate plate and cover plate welded to the bottom ceiling beam to prevent local buckling of the beam plates under the tension forces of the stay bolts. All these manufacturing processes of the modular units can be completed in the factory, and no additional on-site welding is needed.

The cast plug-in unit has four square tube heads on each side of the intermediate connection plate (Fig. 2(b)). During the modular assembly process, the modular column will be inserted in the corresponding head at the plug-in device for alignment. Once the horizontally adjacent modular columns are inserted in place, the modules will be naturally connected together horizontally by the effect of clamping. After the assembly of the modular columns in their correct positions, the long stay bolts will be inserted into the end holes in the beam from the inside of the modular units and fastened to connect the upper floor beam and bottom ceiling beam together. The vertical tension bolts that hold the modules together are hidden behind the base boards in the infill wall; thus, there is no need to create openings that weaken the sections of the structural members, and the gap between the adjacent modules can be small without considering the need for working access.

3. Experimental study

3.1. Description of test specimens and test setup

The connection design was selected from an existing modular office building in Sino-Singapore eco-town in Tianjin Binhai New Area. The office building is a four-story composite modular structure in which the first floor is built with a steel frame structure, and the floors above are constructed using modular units (Fig. 3). The modular units adopted prefabricated concrete slabs in the floor and light weight composite boards for the ceiling, enclosures and partitions of the unit. The floor beams had a comparatively larger section height than the ceiling beams. Although corner-supported modules built and joined with such connections have already been used in practice, the inter-module connections were further modified by using pin connections which cannot transfer moments between the vertically connected unit joints. Therefore, the inter-module connections did not participate effectively in the lateral load resisting system because of the over-conservative designs and lack of knowledge on inter-module connections regarding their actual load transferring behaviours. The aim of the experiments was to study the working mechanism, load bearing mechanism and seismic behaviour of this type of MSB connection in the inner connecting regions. In the actual inner connecting regions, there are four columns and eight beams to be jointed

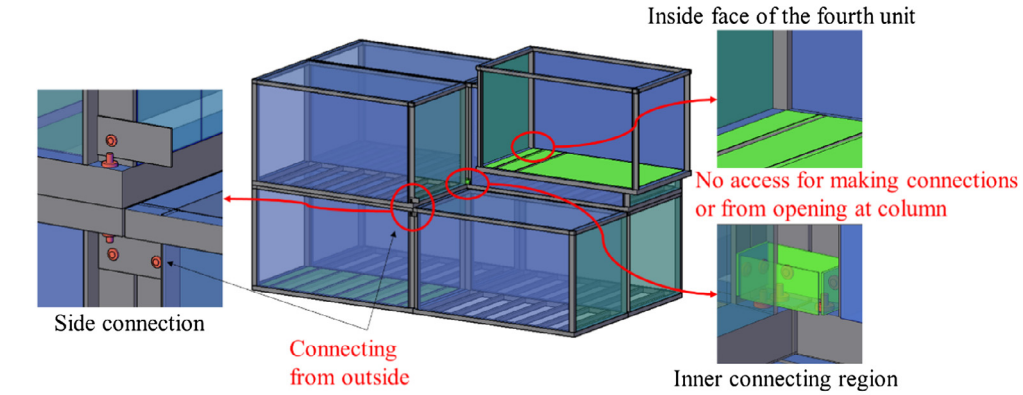

(a) Conventional plate and single bolt connection

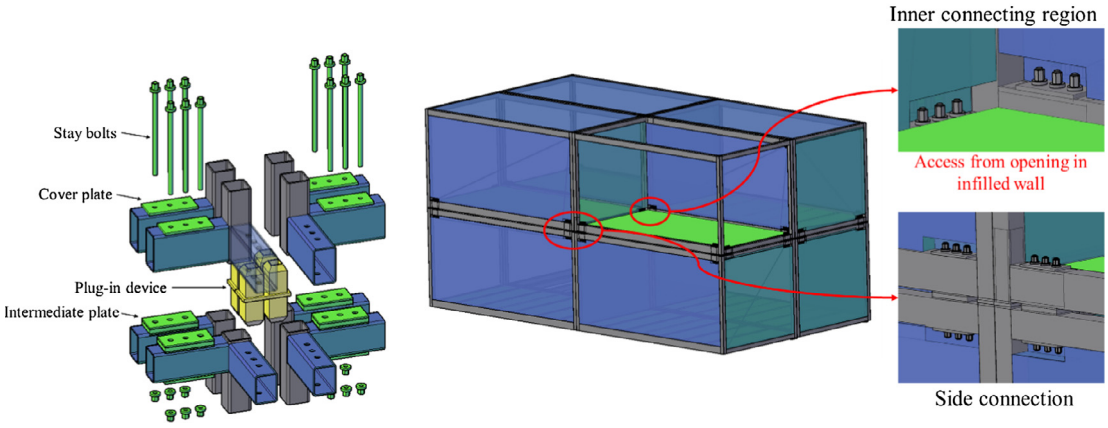

(b) Proposed connection

Fig. 2. Construction of inner connecting region in the proposed MSB connection.

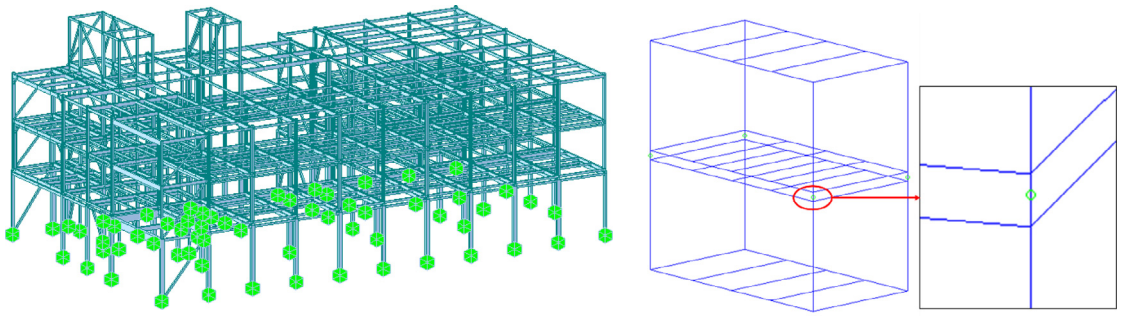

(a) Complete structural model in MIDAS (b) Simplified inter-module pin connection

Fig. 3. Structural model and modular unit composition of the prototype office building.

together, but in the experiments, only a symmetric half was selected as the test specimen, as shown in Fig. 4(a).

During the structural design process, the moment bearing strengths of inter-module connections were designed based on the theoretical moment strength at modular unit joint, i.e., based on the condition when the periphery face of modular column reaches yielding state of the material. The dimensions of the members were designed considering the most heavily loaded inner connection in the modular office building. Owing to testing limitation in the laboratory, the specimens were made with 2/3 scale prototype connections to be consistent with the beam-to-column stiffness ratio. Firstly, two monotonic static loading tests were performed on samples SC1 and SC2 to verify the factor of safety of the design method and to understand the actual load bearing capacity and lateral deforming ability. Two specimens were tested: A base test was conducted on a specimen that had the modular beam welded directly to the modular column, and the other test was on a specimen that had a strengthening connection consisting of two pairs of stiffeners added to the inner side of the upper and bottom unit joints, as shown in Fig. 4(b). Subsequently, four cyclic loading tests were performed on samples QSC1-QSC4 with different dimensions to understand the behaviour of the composite unit and hysteretic performance. The cyclic tests were based on the value of yield strength obtained from previous monotonic test data. The key parameters considered in the tests included the following: (a) effect of diagonal stiffener, (b) unit joint stiffness combinations and (c) axial compression conditions. The information on the specimens is presented in Table 1. Both connections that were

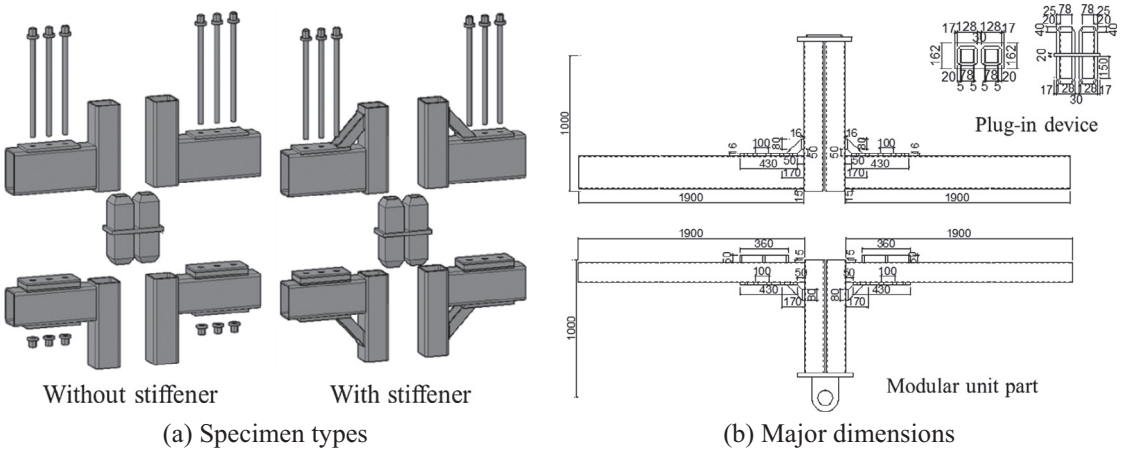

Fig. 4. Detailed information on test specimens.

Table 1
Information on test specimens (with primary varied factor marked in bold in each case).

No.	Ceiling beam (mm)	Floor beam (mm)	Modular column (mm)	Stiffener thickness (mm)	Diameter of bolt (mm)	Axial force ratio	Loading method
SC1	150 × 150 × 8	150 × 250 × 8	150 × 150 × 8	**None**	24	0.2	Monotonic
SC2	150 × 150 × 8	150 × 250 × 8	150 × 150 × 8	10	24	0.2	Monotonic
QSC1	150 × 150 × 8	150 × 250 × 8	150 × 150 × 8	**None**	24	0.2	Quasi-static cyclic
QSC2	150 × 150 × 8	**150 × 150 × 8**	150 × 150 × 8	10	24	0.2	Quasi-static cyclic
QSC3	150 × 150 × 8	150 × 250 × 8	150 × 150 × 8	10	24	0.2	Quasi-static cyclic
QSC4	150 × 150 × 8	150 × 250 × 8	150 × 150 × 8	10	24	**0.1**	Quasi-static cyclic

subjected to monotonic loading had the same dimensions. All the specimens were made of Q345 steel, and used the groove fusion welding for connecting welds. The diagonal stiffeners were connected through fillet welding with wire ER50-6, and as per normal practice, only visual inspection was performed to ensure quality.

All the experiments were performed at the structural laboratory in Tianjin university, with the test setup and measuring arrangement shown in Fig. 5. For testing the connections, column end loading method was adopted, in which an actuator was mounted at the top end of the upper modular column with a 100 t hydraulic jack. Another actuator was mounted at the top end of the upper modular column with a 200 t hydraulic jack to apply the axial load. The axial force in the test was limited to 0.3 times the compressive strength of the modular columns, which is calculated based on yielding condition of all the sections (1.43×10^6 kN). As presented in Table 1, an axial force ratio of 0.2 was adopted in the test (axial force = 286.27 kN); In the case of specimen QSC4, the test was conducted with an axial force ratio of 0.1 (axial force = 143.14 kN), which is half the value for the other tests, for comparison. The top side of the loading jack was bearing against rollers to allow horizontal displacement. Besides, the bottom side of the jack allows slight rotation, and the restraint at the topmost side was assumed to have a free end boundary condition. The axial load was applied up to the designed value before applying the lateral load, and was maintained at the same level throughout the duration of lateral loading. All the beam and bottom column ends were pin constrained to simulate the boundary conditions at moment inflection points. Because of the double beam construction, a special design was needed to ensure a hinged end condition for the beam. As shown in Fig. 5(a), the beam end was constrained by a capping system. Rollers were mounted at the top side of the upper beam, between the floor and ceiling beams, and at the bottom side of the lower beam to allow for independent end rotation and movement of the two modular beams.

Fig. 5(b) shows the displacement measuring plan in which the (W1-W4) are mounted horizontally at the beam and column ends

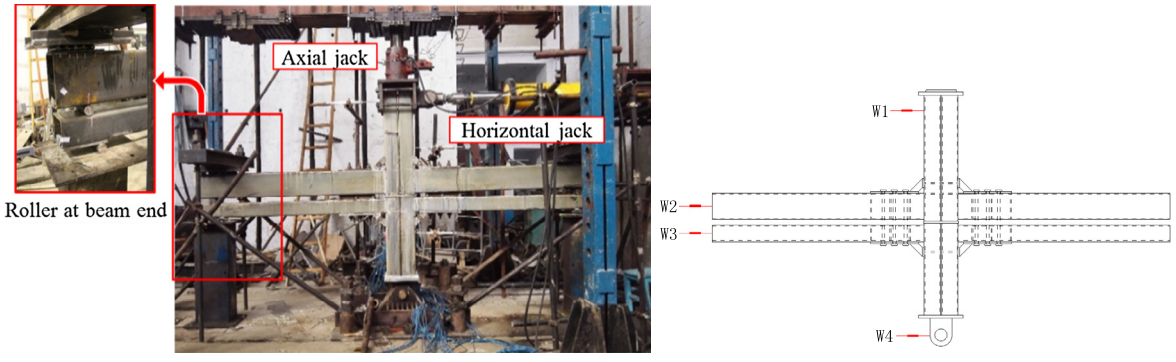

Fig. 5. Test setup and measurement arrangement.

to get lateral displacements at different heights. W1 is located at the top end of the upper column, which is also the loading end, and its value can be used to get the load-displacement relationship for the connection; W2 and W3 measure the horizontal displacements at the ends of the upper floor beam and lower ceiling beam, respectively, and their difference indicates the horizontal dislocation behaviour under lateral loads. In the monotonic loading tests, lateral displacement was applied away from the reaction wall; this direction (towards left) was assumed as the positive loading direction. The quasi-static loading tests were conducted with load-controlled schema with increments of half of the predicted yield strength up to a point before the start of yielding. Once the specimen started yielding or when a clear stiffness reduction was observed, the loading method was changed to displacement-control method with a lateral displacement increment to obtain a yield displacement Δ. Each displacement cycle was repeated twice, and the test was terminated when the axial load could not be maintained or when the lateral force decreased to a value below 85% of the maximum load.

3.2. Results of static monotonic loading tests

Specimen SC1 has a regular inner connection without any stiffening measures. As the lateral load reached 128 kN, a gap began to appear between the two modular columns and the intermediate plug-in device because of the relatively independent construction. As the lateral load is increased, the gap continued to open up. The gap led to uneven transfer of compression load from the intermediate connecting device to the lower modular column, and then led to slight local buckling behaviour at the top end of the bottom modular column. As the lateral displacement reached 88 mm, a sudden loud sound was heard, and a tearing crack occurred at the ceiling beam column joint. With increase in loading, the tearing at the bottom unit joint continued to increase and propagated upward, and the lateral strength continued to decrease. When the lateral displacement reached 132 mm, crack failure occurred at the upper floor unit joint with a significant decrease in lateral strength, and the test was stopped at this instant. Fig. 6(b) shows the deformed state of specimen SC1 at the end of the test; the MSB connection had unequal column inclinations and different joint rotations between the upper and bottom modular parts. The major share of deformation was taken by the bottom joint units.

The dimensions of the members of specimen SC2 are the same as that of SC1, but SC2 had diagonal stiffeners welded at both top and bottom unit joints. Hence, because of the strengthened construction in SC2, the entire connection had a larger lateral stiffness than in the case of SC1, as shown in Fig. 7(a). At a lateral displacement of 25 mm, a gap was observed in the joint region between the upper and bottom modular parts, accompanied by a slight reduction in stiffness in the lateral displacement direction, as shown in Fig. 7(b). On this specimen, a steady increase in strength was observed till the displacement reached 64 mm. At this moment, a local inward extrusion deformation was observed at the compressed bottom joint, which was also accompanied by another reduction in stiffness. When the lateral load reached 398 kN, a loud sound was heard, and brittle facture occurred at the weld between the right bottom stiffener and the column flange (which was in tension state at this moment). Then the test was stopped at this instant. The reduction in strength and the large deformation that occurred during the stiffener failure led to the crack at the weld in the bottom unit joint.

In both the monotonic tests, the results showed similar deformation patterns and failure sequence: gap opening, local buckling at the bottom column ends, and then tearing or brittle fracture at the tension side of the bottom unit joint or local extrusion deformation at the compression side of the bottom joint. In structural design, the inter-module connections are assumed as pin connections which cannot transfer moments. Hence, the overall moment bearing strength would be the sum of the moment strengths for constituent unit joints. The designed lateral force strength was calculated as the sum of the strengths of the two bottom modular columns. The yielding strength of the edge in bending (dotted lines) and the yielding strength of the entire section in bending (dashed lines) are marked in the plot. (the pink lines represent the calculated values based on the designed yield strength of 315 MPa, and the blue lines represent the calculated value based on the yield strength obtained from material tests). The results indicate that for the specimen SC1 with unstiffened connection, the bottom column may barely reach the state of yielding of all the sections, and that its strength is only marginally higher than the designed yield strength. The composite effect of the connection between the unit joints was weak, with the majority of the lateral load and bending deformation being taken by the bottom unit joints. In the case of stiffened specimen SC2, the measured lateral force was higher than the yield strength of the complete section of the bottom column (250.8 kN), indicating that plasticity had developed in the modular columns. The steady load bearing condition between the initiation of the gap and local buckling formation indicates that the vertical stiffener could effectively strengthen the connection and help transfer of the composite load between the assembled joints. Therefore, it can be inferred that the design method with column-controlled bending and the assumption of pin joint for the inter-module connection is applicable for the case of unstiffened connection, but conservative for the stiffened case.

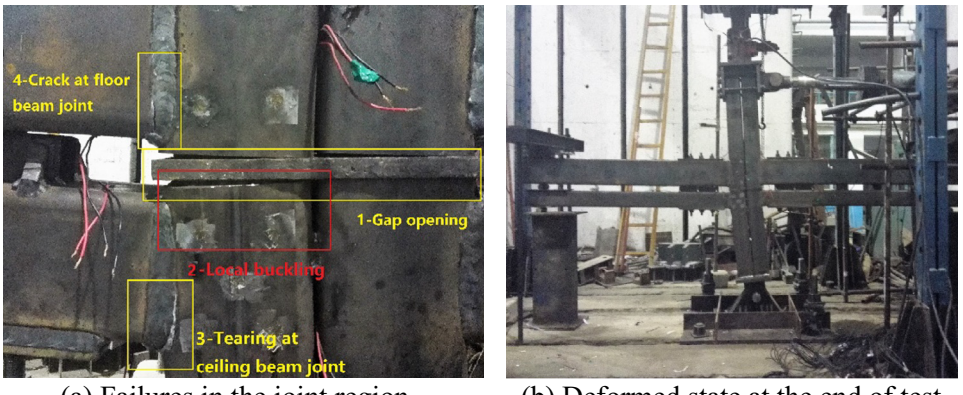

(a) Failures in the joint region (b) Deformed state at the end of test

Fig. 6. Failure mode of specimen SC1.

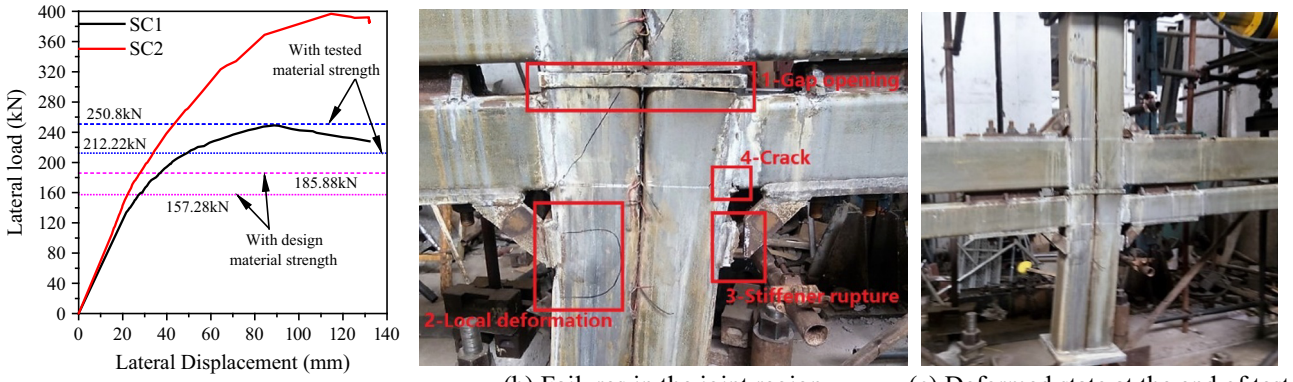

(a) Lateral strength of SC1 and SC2 (b) Failures in the joint region (c) Deformed state at the end of test

Fig. 7. Test results on specimen SC2.

3.3. Discussion of deformation pattern of MSB connection

Fig. 8 shows the deformation mode decompositions of the conventional frame connection, which indicates that the deformation measured at the column tip (Δ) can be decomposed into three components, i.e. flexural rotations of the column (Δc) and the beam (Δb), and the shear distortions in the panel zone (Δj). Thus, in the traditional single beam-single column connection, the column tip displacement Δ and the horizontal displacement D at the beam end would have the relationship shown in Eq. (1). The relationship between the column tip and beam end displacements would be $\Delta > 2D$. However, for the MSB connection, the two displacements have a different relationship.

$$\begin{cases} \Delta = \Delta c + \Delta b + \Delta j \\ D = Dc + Db \end{cases} \begin{cases} \Delta c > 2Dc \\ \Delta b = 2Db \end{cases} \quad (1)$$

Fig. 9 shows the measured displacements and deformation decomposition of the MSB connection. The MSB connection comprises separate upper and bottom unit joints, and each part will have its own joint deformation decomposition as in the case of the frame connection shown in Fig. 8 (Δc1, Δb1 and Δj1 for the upper modular joints and Δc2, Δb2 and Δj2 for the bottom modular joints). Apart from these key factors, there is an additional factor of gap opening at the intermediate jointing region (Δθ) in the MSB connection, which also would influence the overall deforming ability at the loaded tip. Thus, the measured displacements will have following relationships.

$$\begin{cases} W1 = \Delta = \Delta c1 + \Delta b1 + \Delta j1 + \Delta c2 + \Delta b2 + \Delta j2 \\ W2 \approx W3 \approx D = Dc + Db + Dj \\ Dc + Db + Dj \approx \Delta c2 + \Delta b2 + \Delta j2 \\ \Delta c1 = \Delta c - \Delta\theta \end{cases} \quad (2)$$

The measurement W1 represents the sum of upper and bottom modular column deformations. If the beam length variation is ignored, the beam end measurements W2 and W3 could represent the lateral dislocation of the upper and bottom unit joint centres, which result from the deformation at the bottom modular column. Both MSB connections had comparatively large values of W2 and W3, and W1 was smaller than twice the value of D or W3. This deformation patterns and deformation decomposition revealed a separate panel zone deformation between the upper and bottom units, as shown in Fig. 9(d); hence, the comparatively small ceiling beam led to low joint stiffness and a comparatively large bending deformation at the bottom joint. Moreover, the gap would have accommodated part of the bending deformation that was transmitted from the bottom modular unit to the upper one.

4. Results of quasi-static cyclic loading tests

4.1. Specimen performance during testing

Specimens QSC1-QSC4 were subjected to cyclic loading tests to investigate the hysteretic behaviour and energy dissipation performance of the MSB connections. QSC1 had the same construction and axial compression condition as SC1. The specimen showed linear flexural strength-lateral displacement relationship (P−Δ relation) at the beginning of loading. When the displacement at the column tip reached −25.88 mm (Δ), the specimen yielded, and then the loading method was changed to displacement control method. When the lateral displacement reached −50 mm during the second cycle with a displacement of 2Δ, a gap opening was observed between the upper modular column and the intermediate plug-in device, and a slight crack was observed at the tension side of the bottom modular unit joints, as shown in Fig. 10. Besides,

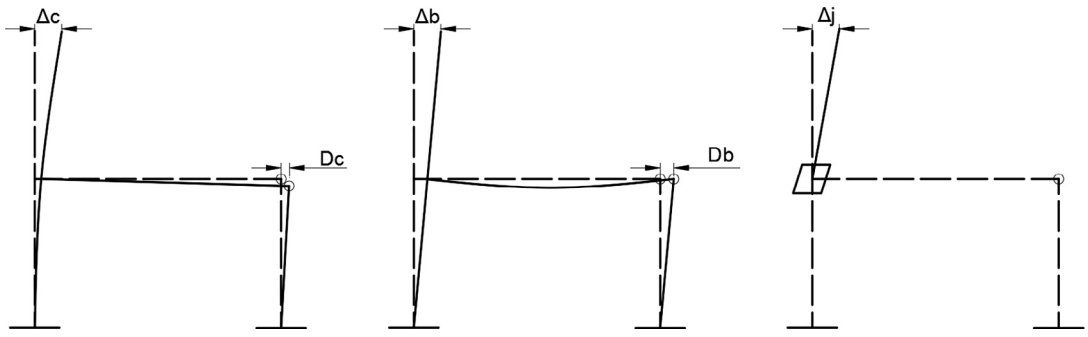

Fig. 8. Deformation decomposition of conventional frame connection.

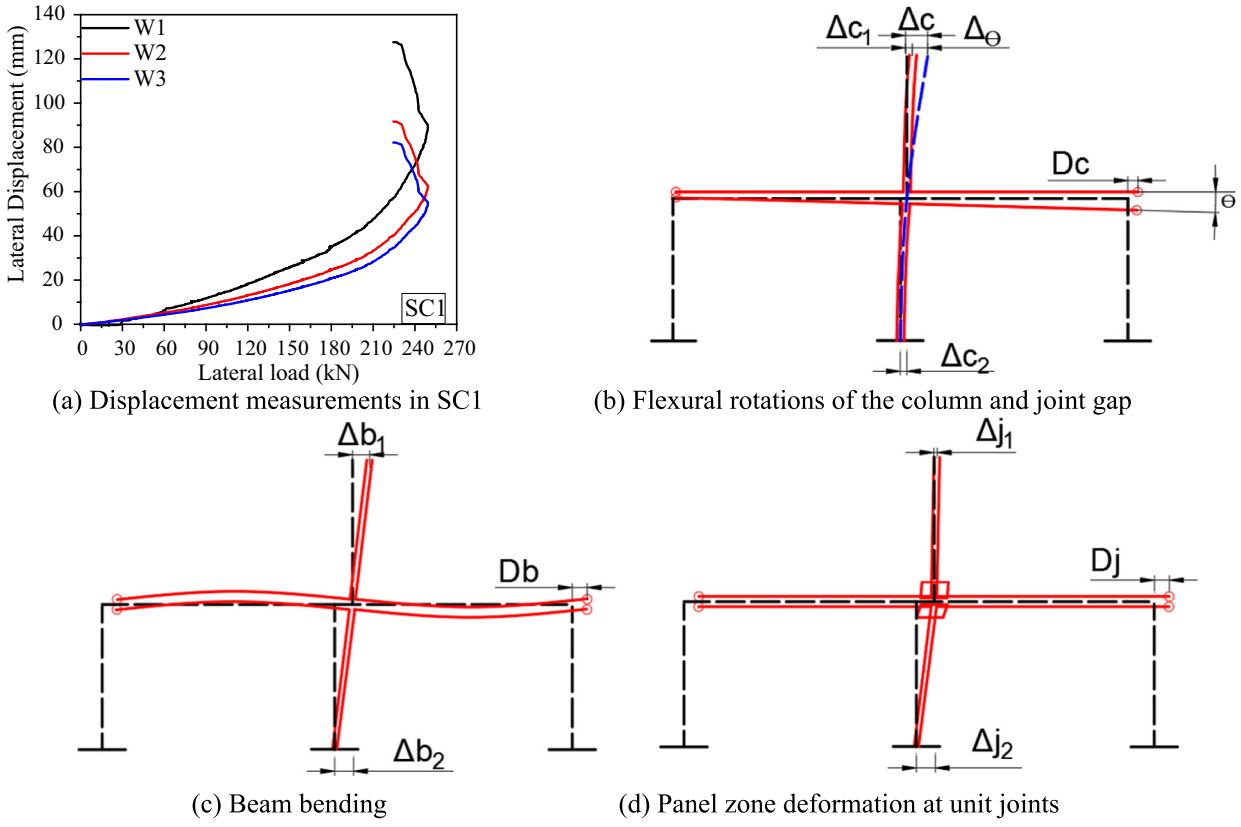

Fig. 9. Deformation pattern and decomposition of MSB connection.

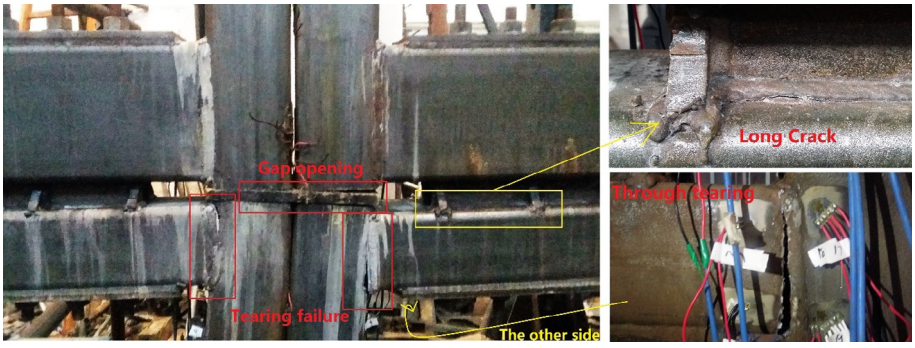

Fig. 10. Failure of QSC1.

long cracks were also observed at the intermediate plate at the long-stay bolting region. In the first cycle with a displacement of 3Δ, the ultimate strength reached 230.6 kN during loading in the negative direction (lateral displacement was −75 mm; positive or negative sign represents the direction), but the strength dropped to 205.6 kN because of gradual tearing at the welds on the beam end of the bottom unit joints during subsequent loading in the reverse direction. When the loaded displacement reached a value of 4Δ, the tearing fracture propagated through the entire ceiling beam height region, and the lateral strength dropped to 171.9 kN, which is approximately 75% of the ultimate capacity (in the negative loading direction). During the subsequent reverse loading, the tearing failure was more severe, and the lateral force dropped to 158.5 kN, which is approximately 77% of the ultimate strength in the positive direction; the test was stopped at this instant.

In the MSB connection design, the floor beams normally have a large section to support the load carrying slab, and the ceiling beams often use smaller section to support the interior fittings and act as temporary support for construction. To compare the effect of unit joint stiffness combinations, specimen QSC2 adopted the same section size for the floor beam as well as for the bottom ceiling beams (Fig. 11). Moreover, this connection had diagonal stiffeners for strengthening. The specimen showed yielding behaviour as the lateral load reached 204 kN at a lateral displacement of −30 mm. Subsequently, loading with displacement control was used with a displacement increment Δ of 30 mm. No change in behaviour was observed before and during loading till 2Δ, but all the floor beams and ceiling beams had visible bending deformation. During the first cycle of loading till 3Δ, small cracks occurred at the plate of the plug-in device. During the second cycle, one stiffener at the right bottom joint fractured when the applied displacement reached −86 mm. Major failures occurred within the period of loading till 4Δ. As the column tip was pulled from 3Δ (90 mm) to −22 mm, another stiffener at the right side fractured.

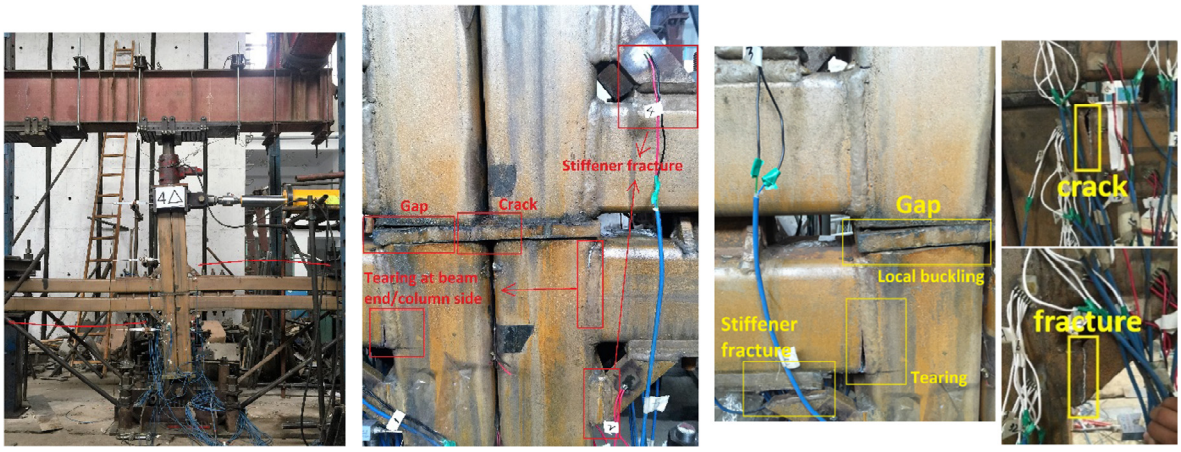

Fig. 11. Failure of QSC2.

When the applied displacement was continued till −110 mm, the column flange at the compression side of the upper joint showed a clear inward deformation. During the process of loading from −4Δ to 4Δ, the stiffeners at the left bottom joints (which are in tension state) fractured subsequently at displacements of 45 mm and 79 mm. Further, during reverse loading from 4Δ to −4Δ, the column flanges had intense buckling, and the crack at the bottom joint spread throughout the ceiling beam. The test was stopped after reaching a lateral load of −283 kN, which is approximately 73% of the ultimate strength.

Specimen QSC3 had the same connection details and axial compression ratio as specimen SC2, and was tested to investigate the hysteretic behaviour. The results are shown in Fig. 12. In this test, the yield load was 243 kN at a displacement of 20 mm (Δ), and the gap opening and local buckling at the bottom column end were visible. Then, during the second cycle of loading till 3Δ, a small crack started in one stiffener at the tension side of the bottom unit joint. As the lateral displacement reached 60 mm, this stiffener fractured. During the process of loading from 3Δ to −4Δ, as the lateral displacement reached −35 mm, one stiffener at the other side fractured. (During the reverse loading process, the stress state changed, and the joint which was previously under compression during bending, changed to a state of tension). Subsequently, as the lateral displacement reached 80 mm (4Δ), the remaining stiffener also experienced rupture failure. After the fracture of most of the stiffeners, the flexural strength of the specimen dropped significantly. Within the process of loading from −4Δ to 5Δ (100 mm), because of the extrusion effect of the stiffener at the compressed region during bending, inward deformation and local buckling occurred at the column flanges. The gap opening increased, and a reduction in strength was observed. The test was stopped after reaching a lateral load of 274 kN, which is approximately 81% of the maximum strength (−335 kN).

Specimen QSC4 had the same construction as specimen QSC3, but was tested with a smaller axial compression ratio of 0.1. This specimen showed a gap opening at the load of 160 kN. When the lateral load reached 240 kN, owing to deficiencies in the clamping system, the foundation experienced a sudden slip and the test was stopped. Slight plasticity was observed in the strength-displacement curves, indicating that yielding had started on this specimen. To understand the factors contributing to the failure, the test setup was reinstalled and the test was continued using a different testing process with displacement control. The displacement increment used was 30 mm. Compared to QSC3, in this specimen (QSC4), fracture failure occurred and propagated into the column flange region of the bottom unit joints (Fig. 13). During the large displacement loading stage, because of the tearing failure at the bottom stiffeners and the resulting reduction in joint bending stiffness, high bending loads were transferred to the upper joints and the corresponding stiffeners, leading to weld crack failures at the upper stiffeners and local deformation due to inward extrusion at the column flanges.

4.2. Deformation pattern during cyclic loading

In all the specimens, different deformation levels and column inclinations between the upper and bottom modular columns were observed. As in the case of the monotonic test, displacement measuring meters were installed horizontally to obtain the inclination patterns in the different parts. Three meters were installed along the vertical column at heights of 2 m (W1), 1.5 m (W2) and 0.5 m (W3) to measure the inclinations of the upper and bottom

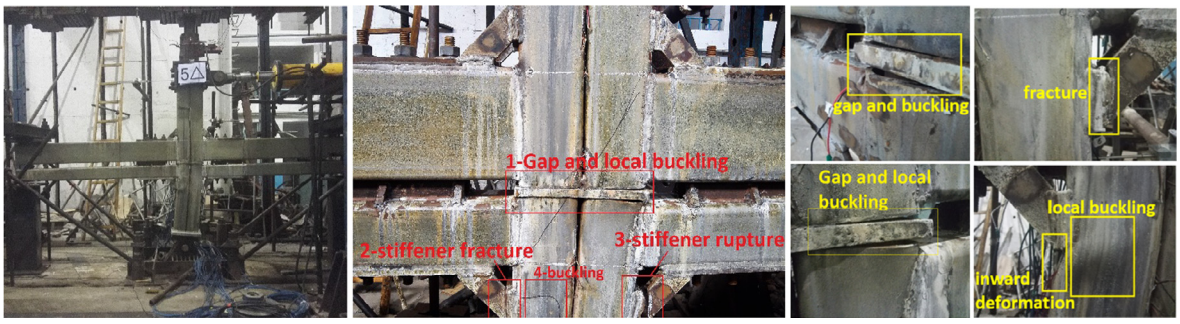

Fig. 12. Failure of QSC3.

Fig. 13. Failure of QSC4.

columns. Because of the operating problems during the test, the full range of data could be obtained for QSC1 and QSC2, as shown in Fig. 14. QSC1 had a large floor beam and no diagonal stiffeners, while QSC2 had welded stiffeners, but a small floor beam size. Fig. 14(a) indicates that larger inclinations occurred at the bottom column than at the upper column, because of the comparatively low bending stiffness of the ceiling beam joints and the higher stiffness of the upper modular parts. Especially in the later loading cycles, because of the fracture or crack failures that happened at the bottom joints, there was a significant reduction in the moment resisting ability, leading to major inclination and bending deformation at the bottom modular joints. In QSC2, both the upper and bottom modular columns showed fairly large column inclinations; however, the inclination at the junction region was small, indicating that the joint stiffness in QSC2 was relatively high, and that the deformation was due to bending at both modular beams and columns.

4.3. Hysteretic performance and skeleton curve

Fig. 15 shows the graph of applied lateral load versus column tip displacement obtained from the quasi-static cyclic loading tests. The overall performance of the MSB connections was similar to that of the conventional frame connections. No obvious pinching was observed from the hysteresis loop, indicating little influence of the gap opening. QSC1 had the smallest flexural bearing capacity, and the ultimate strength was smaller than that for the other three specimens; this difference is mainly attributed to the strengthening effect of the diagonal stiffeners. During the cyclic loading, QSC1 had cracks and tearing at the beam column welds, but the fracture propagation was gradual, and a part of the seismic energy could be dissipated during the testing process. For the stiffened joints, the diagonal stiffeners could effectively protect the welded junction and increase the moment stiffness. However, once the stiffeners were fractured, the sudden loss of stiffness and the release of stored energy might have contributed to the reduction in bending strength of the connection. Hence, when compared to QSC1, QSC3 showed a large connection stiffness and high ultimate strength, but smaller energy dissipation performance and relatively faster deterioration of the connection. The effect of floor beam dimensions can be obtained through a comparison of the results on QSC2 and QSC3. QSC2 had a lower lateral strength, but better energy dissipation than QSC3, indicating that a large floor beam construction can strengthen the connection, but may also lead to a reduction in the deforming ability and ductility of the connection. QSC4 had a similar performance as QSC3, but had a slightly higher ultimate strength, indicating the little influence of axial compression level on flexural bearing capacity. Because of operating problems with the test setup and the selection of a small value of axial compression in the tests, the precise influence of axial compression could not be fully evaluated, and hence further investigations are required.

Fig. 16 shows a comparison of the skeleton curves for the four specimens. The curves reflect the hardening and strength degradation properties of the specimens. Compared to QSC3, QSC1 showed similar initial connection stiffness, but the post-yielding tangent stiffness decreased quickly with a limited level of strength hardening. The comparison indicates that the diagonal stiffeners could help improve the connection stiffness and load bearing strength. Owing to the small floor beam section, QSC2 had low connection

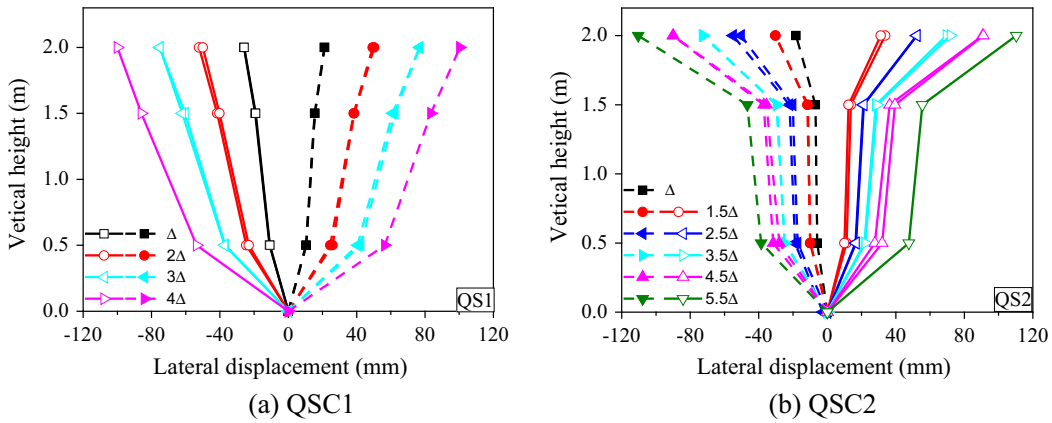

Fig. 14. Deformation pattern on specimens QSC1 and QSC2.

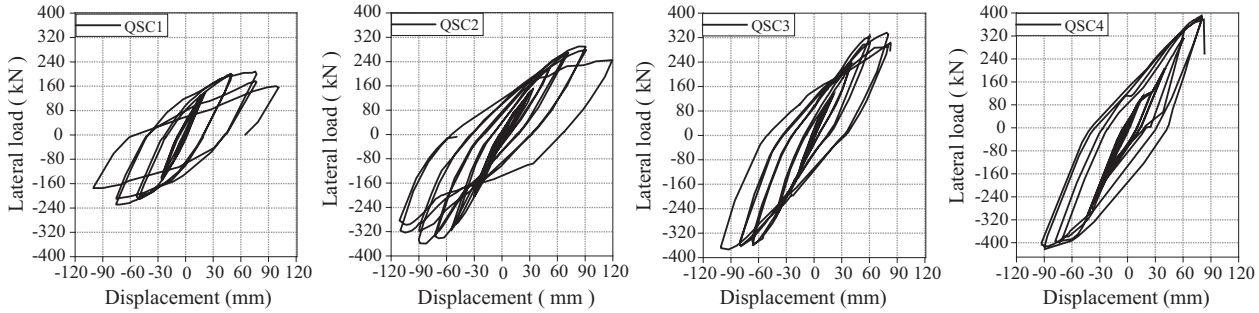

Fig. 15. P-Δ hysteretic relationship.

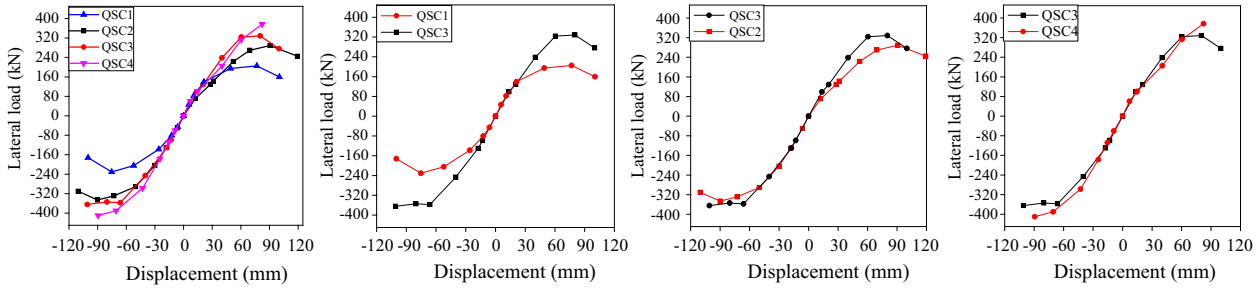

Fig. 16. Skeleton curves.

stiffness, but better deforming ability or ductility of the connection than QSC3. Because of the unexpected situation in the test, only a partial hysterical loop could be obtained for QSC4, and the strength degradation could not be fully obtained. The skeleton curves for QSC3 and QSC4 show a similar trend, and the curve for QSC4 predicts continuous increase in strength even after failure, indicating that a comparatively low axial compression may release a part of the load bearing strength at joint region to moment bearing. But this moment strength elevation effect from axial compression ratio was weak.

4.4. Load bearing and ductility performance

The ductility ratio of the specimens is defined as the ratio of ultimate displacement to the yielding displacement; it indicates the non-elastic deformation capacity without a significant reduction in load bearing capacity. It is an important aseismic index for evaluating the deforming ability of the connection and can be obtained from the hysteretic curve. We define the displacement ductility factor as $\mu = \Delta_{max}/\Delta y$, in which Δ_{max} and Δ_y are the maximum horizontal displacements upon failure and specimen yielding conditions, respectively. Table 2 lists the mechanical factors related to each specimen.

The results showed that the ductility factor was in the range of 2.35–3.42 in all the cases, and that the ratio of ultimate strength to yield strength was in the range of 1.19–1.43 in most of the cases. Most of the ductility factors were greater than 2.5, reflecting the good plastic deforming ability of this MSB connection after yielding. The MSB connection also displayed its promising robustness performance and strength retention ability during degradation

Table 3
Energy dissipation factor and equivalent damping coefficient.

Specimen	Energy dissipation factor *E*	Equivalent damping coefficient *he*
QSC1	2.97	0.47
QSC2	2.16	0.34
QSC3	2.40	0.38

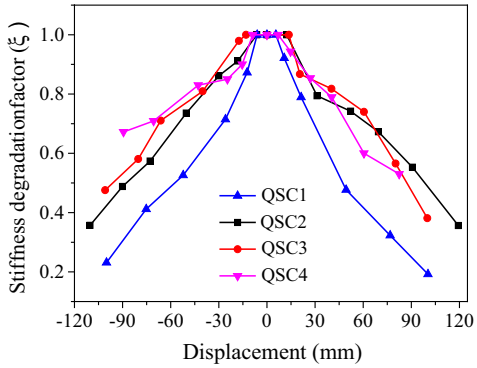

Fig. 17. Stiffness degradation factor.

Table 2
Mechanical factors related to each specimen.

Specimen	Loading direction	P_y (kN)	Δ_y (mm)	P_{max} (kN)	Δ_{max}(mm)	p_u (kN)	Δu (mm)	P_{max} /P_y	μ
QSC1	(+)	154.94	29.34	205.38	76.80	159.72	100.39	1.19	3.42
	(−)	169.78	39.30	230.59	75.25	172.24	100.00	1.38	2.54
QSC2	(+)	206.45	48.01	288.88	90.71	244.79	119.31	1.40	2.48
	(−)	276.80	47.01	346.20	90.06	310.04	110.32	1.43	2.35
QSC3	(+)	186.86	34.89	328.39	80.23	276.01	100.00	1.27	2.87
	(−)	216.85	39.62	364.54	80.25	354.53	100.85	1.37	2.55

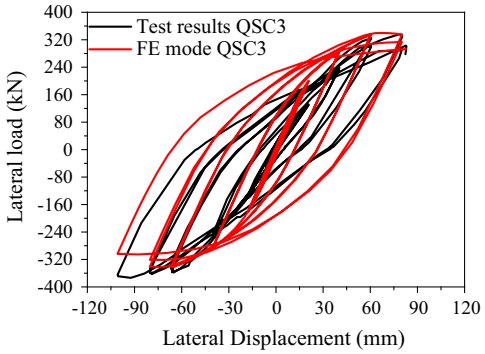

Fig. 18. Verification of finite element simulation.

process. In the conventional single-column single-beam frame connection, once fracture happens at the beam end welds or stiffener ends, the lateral strength would decrease quickly. However, in the MSB connection, most of the weld fractures occurred during the process of cyclic loading to 3Δ, and there were tearing cracks of full height at the ceiling beam joints in some cases, but the lateral bearing strength of the entire connection could still be maintained with a steady decreasing trend, without a sharp drop in strength. Even with the breakage of the ceiling beams, the beams or slabs did not collapse because of the separate floor beam (slab) and ceiling beam (slab) construction, and the use of stay bolts for fastening the beam-to-beam assembly.

4.5. Energy dissipation

The energy dissipation factor is another important indicator for aseismic performance. This can be measured as the area enclosed by the force–displacement hysteresis loop. A plump hysteresis loop or a large enclosed loop area represents good energy absorption ability and better aseismic behaviour. There are normally two coefficients to describe the energy absorption performance: energy dissipation factor E and equivalent damping coefficient he. A large

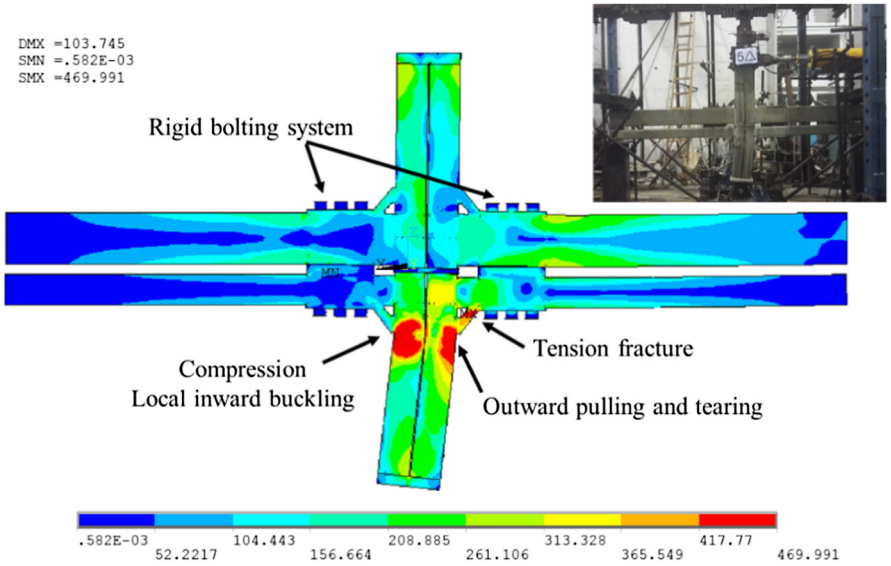

(a) Negative 5Δ displacement state (displacement at -103.7 mm)

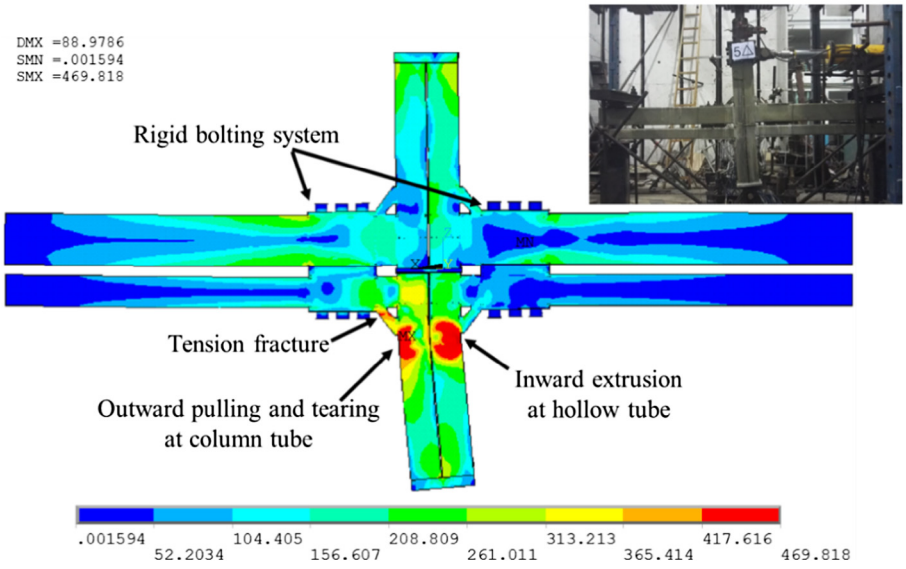

(b) Positive 5Δ displacement state (displacement at 89 mm)

Fig. 19. Von Mises stress distribution in QSC3 (stress unit in MPa).

value of *E* or *he* indicates better energy dissipation ability and good aseismic performance. A detailed calculation method can be found in Ref. [15]. The energy dissipation capacity of the specimens increased steadily with increase in the displacement amplitude in the hysteresis loop up to the failure point; the values of the two factors, obtained from the last loop are presented in Table 3. Although QSC1 had a comparatively lower lateral strength, the failure mode was gradual weld tearing at the unit joints, leading to more energy dissipation and high *he* coefficients. The final equivalent damping coefficients of specimens QSC1, QSC2 and QSC3 were 0.47, 0.34 and 0.38, respectively. Compared to the values for a concrete connection, whose equivalent energy damping coefficient is $0.1 \sim 0.2$ for the centre joints, the proposed MSB connections have more than twice the energy absorption level, indicating a reasonably good aseismic ability.

4.6. Stiffness degradation

Stiffness deterioration is defined as the reduction in tangent stiffness of the connection under cyclic loading conditions such as earthquake ground motions. Normally, stiffness degradation factor (ξ) is defined as the ratio of scant stiffness at each loading amplitude to the initial stiffness (K_0). Fig. 17 shows the stiffness degradation of each specimen during the cyclic loading test. During the initial cycles, there was no significant degradation in stiffness for all the specimens. As the connections entered the yielding and plastic state, the specimens deteriorated at different rates. QSC1 had the most significant stiffness reduction rate, while the stiffened specimens had a more gradual decrease in stiffness. Both QSC3 and QSC4 showed similar deterioration trends; these connections had a high rate of stiffness reduction after yielding, which mostly corresponds to the moment of the first occurrence of a fracture or crack. Subsequently, the deterioration slowed down during the gradual tearing and subsequent rupture process. Overall, for this MSB connection design, the factors influencing the lateral bearing strength and stiffness can be ranked in the following order: diagonal stiffeners, modular beam section combinations and axial compression levels.

5. Numerical analysis

For a better understanding of the internal stress distribution within the MSB connection components, a finite element (FE) model was established for specimen QSC3 using ANSYS program. To get a more refined and accurate simulation, solid element SOLID95 was used for all the steel parts, including the modular members, intermediate connecting device and long stay bolting systems. Contact pair CONTA174 and TARGE170 elements were used at the contacting surfaces between the plug-in device and modular tubes to simulate the assembled relationship, and between the long stay bolts and cover plates to study the bolting and sliding conditions. Three linear kinematic material models were adopted for the steel materials, with the critical points defining the stress-strain relationship set according to the measured data from material coupon tests.

A comparison of the lateral load-column tip displacement hysteretic curves is shown in Fig. 18. The initial stiffness obtained from the FE analysis was slightly larger than that obtained from the experiments, but the later values of stiffness and strength increase were consistent with experimental results. The pinching phenomenon in the hysteretic curves determined from the FE analysis for QSC3 was not as significant as that found in the experimental results. Such a discrepancy between the hysteretic curves obtained from the experiments and FE analysis for QSC3 may be attributed to the microgaps within the assembled MSB connection. However, the loading capacity obtained from the analysis compared reasonably well with that obtained from the experiments.

Fig. 19 shows the Von Mises stresses in specimen QSC3 during the last loading cycle (5Δ), and the measured strain data and variation at each load level are plotted in Figs. 20 and 21. The predicted deformation pattern and stress distributions were consistent with the test results. For specimen QSC3, high stress were concentrated mainly at the bottom joint region, especially at the diagonal stiffeners and their connection to the bottom modular columns. Because of the small and hollow section of the modular columns, the large deformation led to high tension and compression forces at the bottom stiffeners; these forces were induced by the high tearing and local extruding pressure at the bottom column flanges. The stress level at the beam end joints remained at a comparatively low level, indicating the strengthening effect of the diagonal stiffeners. The assembled composition and gap between the upper and bottom modular parts relieved the bending deformation. Thus, together with the comparatively rigid bending stiffness at the upper floor beam joints, the overall stress levels remained at reasonable levels. The joint region of the entire specimen showed a combined effect of individual bending of each unit joint together with the composite effect as an assembled junction. As shown in Fig. 19, the upper welds at the ceiling beam ends also showed very

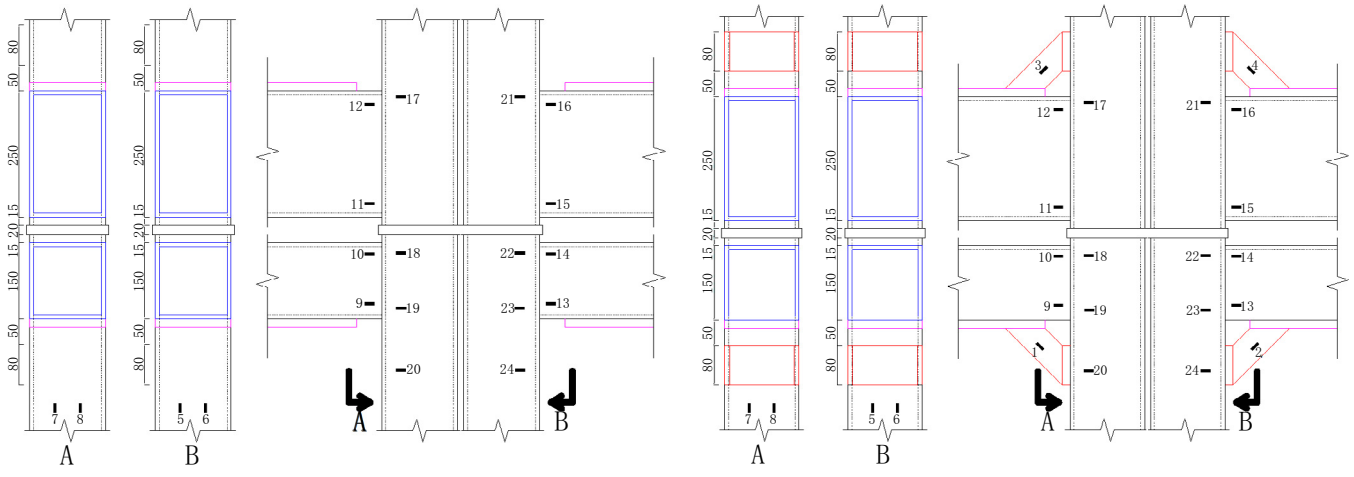

(a) Strain distribution in QSC1 (b) Strain distribution in QSC2-QSC4

Fig. 20. Strain gauge locations.

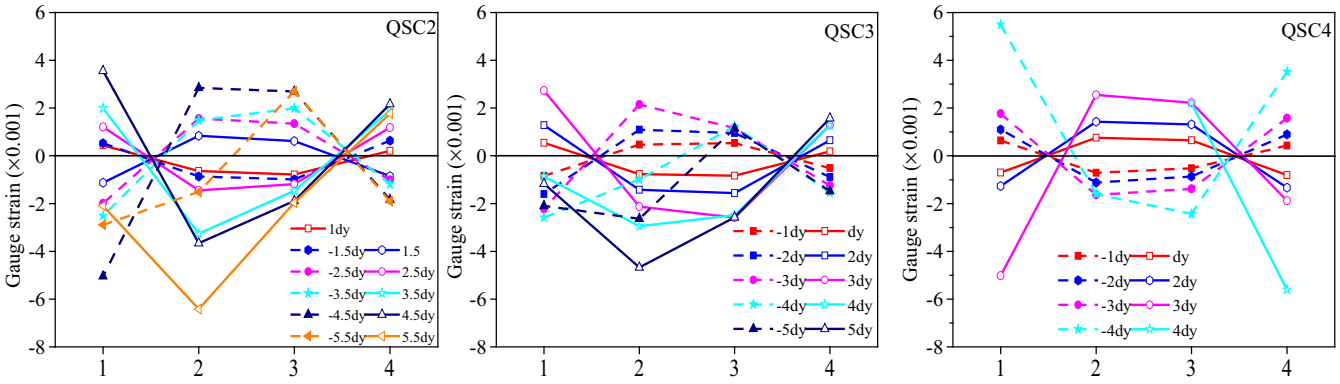

(a) Strain distribution at diagonal stiffeners

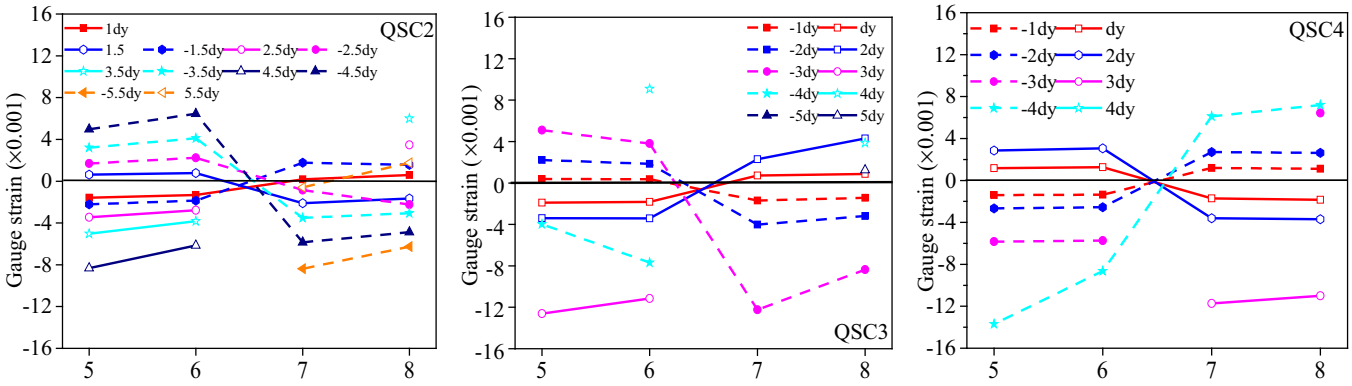

(b) Strain distribution at column flanges

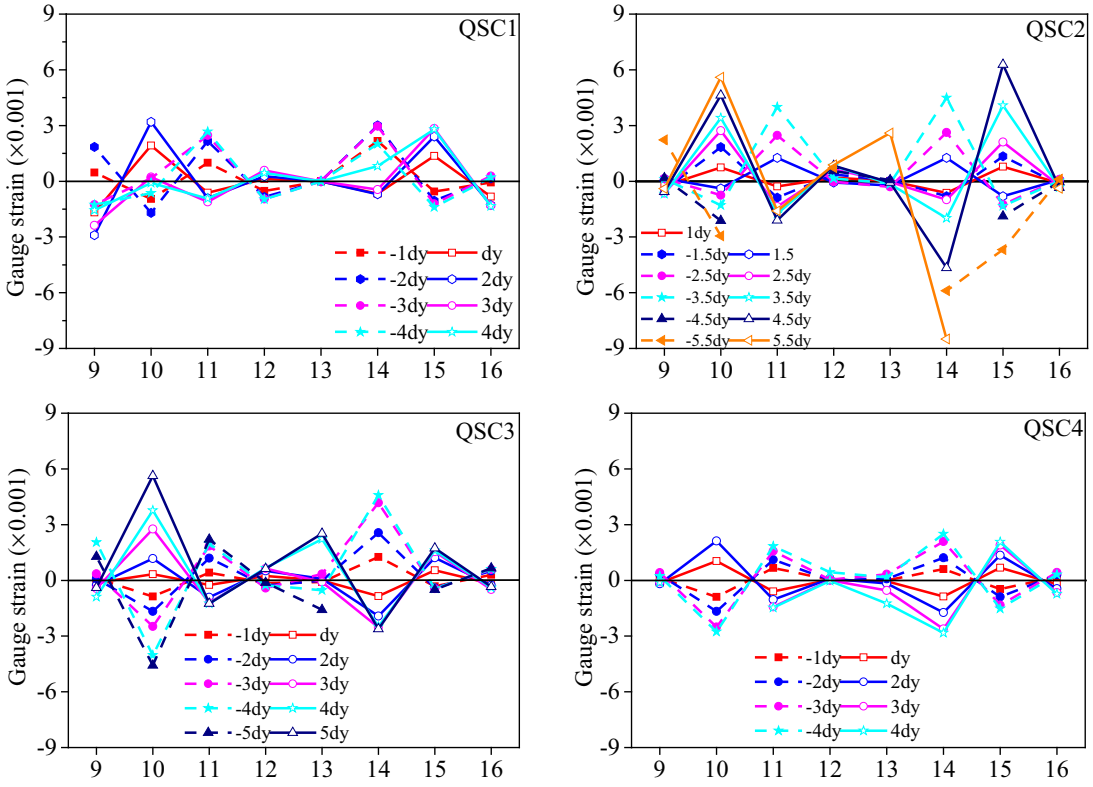

(c) Strain distribution at beam ends

Fig. 21. Measured strain conditions.

high stress levels, corresponding to the crack failures at these locations during the test. Moreover, because of the strengthening effect of the cover plates, the beam-to-beam connecting region formed a rigid zone and a relatively low stress level was maintained.

Fig. 21 shows the strain variations in the different specimens. QSC2 and QSC4 had higher stresses than QSC3 at locations like both diagonal stiffeners and column flanges. However, the influencing mechanisms were different. The small floor beam section in QSC2 reduced the moment bending percentage at beams but increased the stress demand at the joint regions, while the high stresses in QSC4 mainly resulted from the larger column inclination and the large induced deformation of the joint under low compression levels. Fig. 20(c) shows a comparison of the stress states in the beam end regions. QSC1 had a high strain at both sides of each unit beam end, and shows the typical bending stress distribution in the moment joint. Because of the smaller section at the ceiling beam, the bottom column had higher internal stresses at the joint region than the upper column. All the stiffened specimens QSC2-QSC4 had large strains at gauge locations 10, 11, 14 and 15, and very low strains at gauge locations 9, 12, 13 and 16; this shows the individual participation of each unit joint in bending and the strengthening effect of the diagonal stiffeners. Furthermore, at the beam end regions, large strains were still developed in QSC2. Hence, in the MSB connection design, special attention is needed not only to the safety of the unit joints, but also to the relative stiffness and the composite effect between the assembled joints.

6. Conclusion

This paper proposed a new design of an inter-module connection for modular steel buildings. Systematic experiments, including two monotonic loading and four quasi-static cyclic loading tests, were performed on the inner MSB connections to study the load bearing mechanism and aseismic behaviour. FE simulation was also conducted to help understand the stress development and distribution patterns in the MSB connections. The conclusions are given below.

(1) The proposed MSB connection is superior to the traditional connector plate and single bolt connection in terms of convenience of erection at site, especially for the connecting regions in the inner modules. The beam-to-beam bolted connection can be accessed through the infill wall, the gap between the adjacent modules can be small without considering the working access for the connections.
(2) All the stiffened and unstiffened specimens failed in the monotonic loading tests by tearing at the tension side of the bottom joint or local extrusion deformation at the compression side of the bottom column. The MSB connection allowed separate deforming extent between the upper and bottom units, with the major column inclination and joint rotational deformation occurring in the bottom units. The design method with the assumption of a pin joint at the inter-module connection was applicable for the case of unstiffened connection, but was conservative for the stiffened case.
(3) The deformation patterns, failure modes, lateral strength improvement, and energy dissipation abilities of the inner MSB connections were closely related to the bending stiffness of each unit joint and their relative stiffness. The diagonal stiffeners could increase the bending stiffness and lateral bearing strength. However, they caused a reduction in energy dissipation and resulted in the relatively rapid deterioration of the connection once the stiffeners fractured. Because of the double columns, double beams and their construction using long stay bolts, even with severe tearing and fracture that occurred in the connection, there was no collapsing of the structure.
(4) The strain distributions obtained from the measurements and FE simulations revealed that all the unit beams and joints had independent and individual bending behaviours instead of ideally working together as a composite large beam or united connection. The ceiling beam end joints were found to be the critical parts.

Acknowledgements

This research was sponsored by the National Nature Science Foundation of China (Grant No. 61272264), Project of Tianjin Urban & Rural Construction Commission (2013E3-0028) and China Postdoctoral Science Foundation (2016M590202).

References

[1] Lawson RM, Ogden RG, Bergin R. Application of modular construction in high-rise buildings. J Arch Eng 2012;18(2):148–54.
[2] Fathieh A, Mercan O. Seismic evaluation of modular steel buildings. Eng Struct 2016;122:83–92.
[3] Gibb A, Isack F. Re-engineering through pre-assembly: client expectations and drivers. Build Res Inf 2003;31(2):146–60.
[4] Annan CD, Youssef MA, El-Naggar MH. Effect of directly welded stringer-to-beam connections on the analysis and design of modular steel building floors. Adv Struct Eng 2009;12(3):373–83.
[5] Lawson M, Ogden R, Goodier C. Design in modular construction. CRC Press; 2014.
[6] Lawson RM, Richards J. Modular design for high-rise buildings. Proc Inst Civ Eng Struct Build 2010;163(3):151–64.
[7] Lawson P, Byfield M, Popo-Ola S, Grubb P. Robustness of light steel frames and modular construction. Proc Inst Civ Eng Struct Build 2008;161(1):3–16.
[8] Lawson RM, Ogden RG. 'Hybrid' light steel panel and modular systems. Thin-Walled Struct 2008;46(7–9):720–30.
[9] Lee S, Park J, Kwak E, Shon S, Kang C, Choi H. Verification of the seismic performance of a rigidly connected modular system depending on the shape and size of the ceiling bracket. Materials 2017;10(3):263.
[10] Annan CD, Youssef MA, El Naggar MH. Experimental evaluation of the seismic performance of modular steel-braced frames. Eng Struct 2009;31(7):1435–46.
[11] Annan CD, Youssef MA, El Naggar MH. Seismic vulnerability assessment of modular steel buildings. J Earthquake Eng 2009;13(8):1065–88.
[12] Fathieh A, Mercan O. Three-dimensional, nonlinear, dynamic analysis of modular steel buildings. Struct Congr 2014;2014:2466–77.
[13] D. Farnsworth, Modualr tall building design at Atlantic Yards B2, Proceedings of CTBUH 2014 International Conference, Shanghai, China, 2014, pp. 492–499.
[14] S. Mills, D. Grove, M. Egan, Breaking the prefabricated ceiling challenging the limits for modular high rise, Proceedings of CTBUH 2015 International Conference, New York, USA, 2015, pp. 416–425.
[15] Qin Y, Chen Z, Yang Q, Shang K. Experimental seismic behavior of through-diaphragm connections to concrete-filled rectangular steel tubular columns. J Constr Steel Res 2014;93:32–43.